Journal of Ultrafine Grained and Nanostructured Materials
https://jufgnsm.ut.ac.ir
Vol. 52, No.1, June 2019, pp. 57-68
Print ISSN: 2423-6845 Online ISSN: 2423-6837
DOI: 10.22059/JUFGNSM.2019.01.06

Effect of pulsed current densities on co-electrodeposition of Graphene Oxide/ Calcium-Phosphate coatings and their biocompatibility

Leila Fathyunes*[*,1], Jafar Khalil-Allafi[2], Fatemeh Marashi-Najafi[2]

[1]*Department of Materials Science and Engineering, University of Bonab, Bonab, Iran.*

[2]*Research Center for Advanced Materials, Faculty of Materials Engineering, Sahand University of Technology, Tabriz, Iran.*

Recieved: 23 December 2018; Accepted: 17 March 2019

** Corresponding author email: Fathyunes.metallurgy@gmail.com*

ABSTRACT

In this study, calcium-phosphate (Ca-P) and graphene oxide (GO)/ calcium-phosphate (Ca-P) coatings were electrodeposited with different pulsed current densities on TiO_2 nanotubes. Results showed that the co-electrodeposition rate in the presence of GO, especially at low current densities of 2 and 5 mA/cm^2, significantly decreased. This might be due to the large size of GO sheets as compared to the size of calcium and phosphate ions. The SEM micrographs revealed that the surface of the anodized titanium could not be completely covered with the GO/Ca-P coatings applied at such low current densities. However, producing a considerable amount of H_2 gases at higher current densities of 10 and 15 mA/cm^2 caused the formation of a coating with poor quality. Regarding this, increasing the off part of the pulsed current by changing duty cycle from 0.3 to 0.1 led to the co-electrodeposition of GO/Ca-P coating with an acceptable quality. The FTIR and micro-Raman analyses also demonstrated that the current density of 15 mA/cm^2 was more favorable to apply the coating predominantly consisting of hydroxyapatite (HA) phase. At last, studying the ability of apatite mineralization in simulated body fluid (SBF) displayed that both Ca-P and GO/Ca-P coatings electrodeposited at the current density of 15 mA/cm^2 and duty cycle of 0.1 are acceptable for biomedical applications.

Keywords: *Calcium Phosphate, Graphene Oxide, coating, Pulsed current densities, Co-electrodeposition, Biocompatibility.*

1. Introduction

The population aging, increasing high-risk activities, and bone injuries have led to a growing worldwide demand to replace the lost or infected biological structures [1]. Titanium because of having the elastic modulus close to that of bone, high strength-to-weight ratio, biocompatibility, high corrosion resistance and low toxicity, has attracted significant interest as dental or orthopedic implants [2,3]. However, this bio-inert metal is usually encapsulated by the host organisms, and therefore, is loosened at the interface with the bone [4]. To overcome this drawback, the metallic implants are often coated with biomaterials such as hydroxyapatite (HA) [1,4,5]. However, the inherent brittleness of HA restricts its clinical applications, especially under mechanical loadings [6]. One approach to solve this problem is using the graphene or its derivatives as reinforcement in the HA matrix [7–9]. Among the various methods available for applying the HA coatings, the electrodeposition has some advantages including good control of the

coating composition and thickness, as well as the ability to form the coating on complex or porous shapes [10,11]. Nevertheless, the evolution of H2 gases in this method deteriorates the quality of coating and its adhesion to the substrate. To overcome these obstacles, using the pulsed current would be useful [12,13].

Besides, the incorporation of particles as second phase into the coating by co-electrodeposition process and quality of the obtained composite coating is dependent on many parameters such as concentration of particles in the electrolyte, surface charge and size of these particles and surely the applied current density [14,15]. Formation of the uniform coatings with suitable adhesion to the substrate is crucial for biomedical applications. Therefore, the main goal of this work is co-electrodeposition of the GO/Ca-P composite coating with satisfactory quality on the anodized titanium using pulsed current densities. For this purpose, optimization of the current density and the duty cycle has been done. Moreover, a comparative study has been performed on the microstructure, biocompatibility and chemical phases of the Ca-P and GO/Ca-P coatings electrodeposited under same conditions. It is worth noting that the results of further studies about the mechanical properties, cellular behavior and corrosion resistance of the GO/Ca-P composite coating electrodeposited at the optimized current density and duty cycle have been presented in our recently published papers [8,16].

2. Experimental

2.1. Development of Ca-P and GO/Ca-P coatings on the anodized titanium

The pure titanium samples (99.9%, Grade 1) with size of 10×10×1 mm^3 were mechanically polished using SiC papers ranging from P120 to P5000 grit and then were chemically polished in HNO_3/HF (1:3 in volume ratio) solution for 30 s. The edges and backside of the titanium substrates were sealed by epoxy resin so that only their front face with the surface area about 1 cm^2 was exposed to the electrolyte. The samples were ultrasonically cleaned in acetone, ethanol and deionized water, respectively. Before applying the Ca-P based coating, anodizing of titanium was carried out in ethylene glycol based electrolyte at a constant voltage of 60 V [8].

The electrolyte for electrodeposition of the Ca-P based coatings was an aqueous solution containing 0.042 M $Ca(NO_3)_2$, 0.025 M $NH_4H_2PO_4$ and 6 mL/L H_2O_2. The pH and temperature of this electrolyte were adjusted to 4.5 and 65±2 °C, respectively. To apply the GO/Ca-P coating, 100 µg/mL of GO was also added to above electrolyte. It should be mentioned that, the GO sheets were synthesized according to the modified Hummer's method [12,16]. Prior to the co-electrodeposition, the above electrolyte was ultrasonically treated for 20 min. A magnetic stirring of the electrolyte was also maintained at a speed of 120 rpm during electrodeposition. The anodized titanium as a cathode and graphite as an anode were set at a fixed distance of 2 cm. The GO/Ca-P and Ca-P coatings were electrodeposited at the pulsed current densities of 2, 5, 10 and 15 mA/cm^2 with two different duty cycles of 0.3 and 0.1.

2.2. Characterization

The surface morphology of the anodized titanium and coatings was observed by scanning electron microscope (Cam Scan MV2300-Czech) coupled with an energy dispersive spectroscopy (EDS).

The weights of Ca-P and GO/Ca-P coatings were obtained through measuring the weight of the anodized titanium before and after electrodeposition at the duty cycle of 0.3 and 0.1 and current densities of 2, 5, 10 and 15 mA/cm^2.

The bonding strength of coating to anodized titanium was evaluated according to the ASTM F1044-05 standard, using a Universal testing machine (model: Santam STM50) at a constant crosshead speed of 1 mm/min.

The structure of graphite and GO was analyzed by X-ray diffraction (XRD, BRUKER-D8 Advance-Germany Spectrometer) with Cu K_α radiation, the step size of 0.03° and the step time of 1s.

Transmission electron microscopy (TEM) image of the GO sheet was collected using a Philips CM30 system operating at 150 kV.

The chemical bands of the powder scrapped from coatings and the synthesized GO were studied by Fourier Transform Infrared Spectroscopy (FT-IR, BRUKER) between 400 and 2000 cm^{-1}.

The micro-Raman spectra of the coated samples were recorded using SENTERRA-BRUKER Germany spectrometer with a 532-nm laser source in the range of 300-1800 cm^{-1}. Since fluorescence background is a serious challenge in the Raman analysis of apatite, the samples before the analysis were subjected to 30 minutes photo-bleaching.

At last, in order to compare the apatite mineralization ability of the coated samples, they were immersed in 20 mL of simulated body fluid (SBF) and then were stored in an oven at 37 ˚C for 7 days.

3. Results

Fig. 1 shows the top-view SEM image of the porous TiO_2 layer formed by anodizing on the titanium surface. As mentioned in the introduction part, electrodeposition is an attractive method to apply the Ca-P coatings, however, improving the adhesion of the coatings obtained by this method to the titanium substrate is necessary for clinical applications. Introducing an intermediate layer such as TiO_2 can be a favorable way for this purpose [1,4]cell differentiation, and enhancing osseointegration.

Figs. 2 (a) and (b) present XRD pattern and TEM image of the synthesized GO. The GO sheets exhibit a distinct diffraction peak at 2θ:10.35˚ corresponded to (001) reflection. Moreover, the transparent and wrinkled sheet can be seen in TEM image, indicating the well exfoliation of graphite oxide into few-layered graphene oxide (GO).

Fig. 3 shows variations in the weight of the Ca-P and GO/Ca-P coatings electrodeposited at the current densities of 2, 5, 10 and 15 mA/cm^2 and the duty cycle of 0.3 (t_{on}:1s and t_{off}: 2s) for 30 min. As it is clear, the weight of the Ca-P based coatings decreases in the presence of GO sheets. Increasing the current density up to 15 mA/cm^2 results in achieving a higher co-electrodeposition rate for the GO/Ca-P coating. Under this condition, the differences between the weight of the Ca-P and GO/Ca-P coatings reduce, so that the measured values are close to each other. However, the weight of the composite coating is still lower than that for the Ca-P coating.

Moreover, SEM images show that the fully

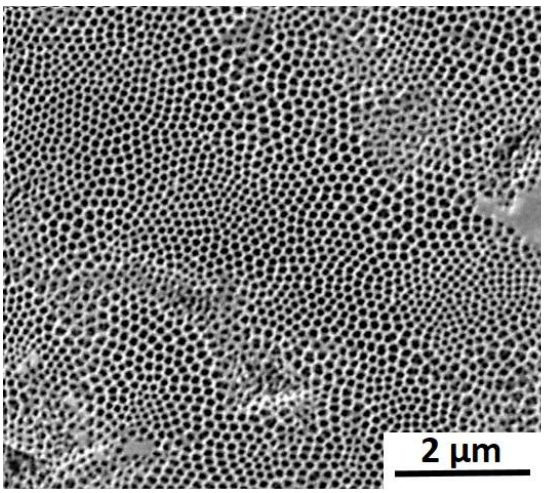

Fig. 1- Top-view SEM image of TiO_2 layer formed on the anodized titanium.

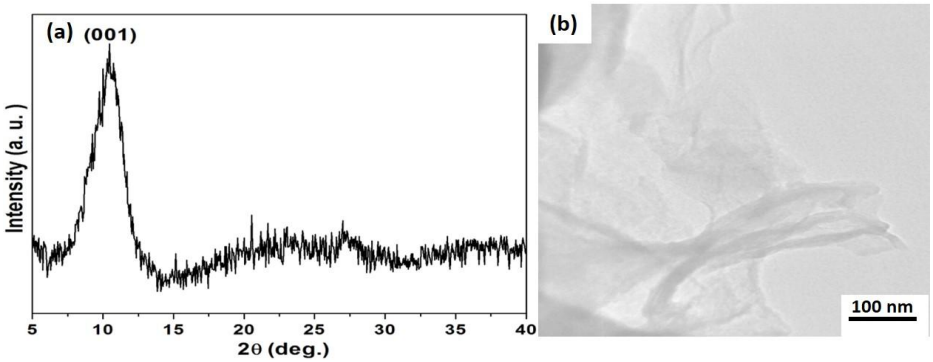

Fig. 2- The synthesized GO. (a) XRD pattern and (b) TEM image.

covered Ca-P coatings could be formed by electrodeposition at low current densities of 2 and 5 mA/cm^2 (see Figs. 4 (a and b)). While, there is a large difference in the coverage capability of the GO/Ca-P coating. To support the above statement, Figs. 4 (c and d) show remaining some uncovered areas throughout the coated surface (marked by the yellow circles), whereas the GO/Ca-P composite coating was co-electrodeposited at 2 and 5 mA/cm^2. This might be related to the fact that presence of GO sheets in the electrolyte reduces the rate of the coating formation. Hence, existence of these uncovered areas on the GO/Ca-P coated sample results in a significant difference between the weights of the composite coatings and the Ca-P ones applied at such low current densities (see Fig. 3).

Moreover, despite increasing the co-electrodeposition duration to 60 min, the surface coverage with the GO/Ca-P coating applied at 5

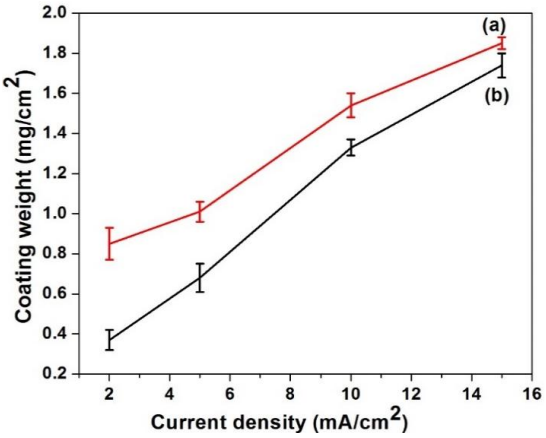

Fig. 3- Variations in the weight of the Ca-P and GO/Ca-P coatings applied at the different current densities and the duty cycle of 0.3 for 30 min.

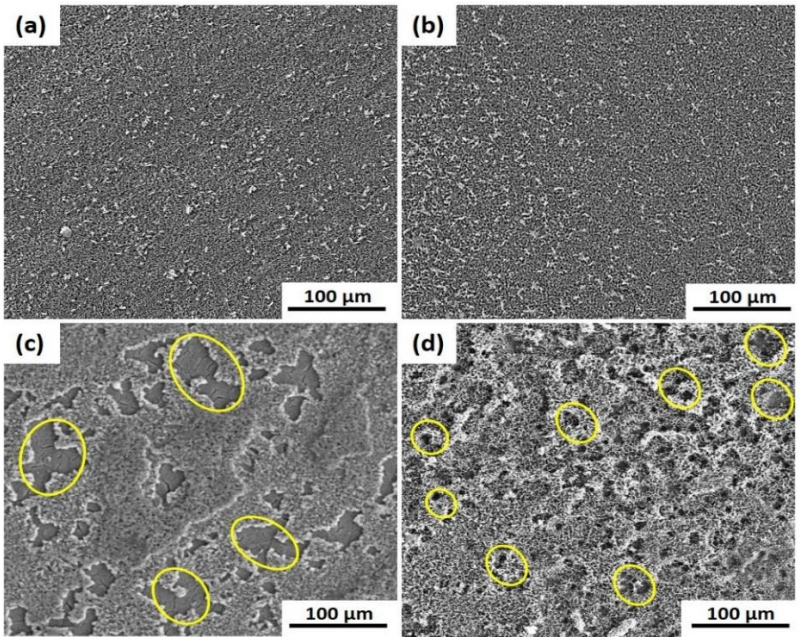

Fig. 4- The SEM micrographs of coatings electrodeposited for 30 min at the duty cycle of 0.3: (a) Ca-P; 2 mA/cm^2, (b) Ca-P; 5 mA/cm^2, (c) GO/Ca-P; 2 mA/cm^2, and (d) GO/Ca-P; 5 mA/cm^2.

mA/cm^2 and duty cycle of 0.3 is still poor and some uncoated areas are distinguished on the surface (Fig. 5, yellow circles). Regarding this challengeable issue, it seems that a higher current density is necessary to obtain the GO/Ca-P composite coating with better coverage capability.

The SEM images in Fig. 6 show that the co-electrodeposition at high current densities of 10 and 15 mA/cm^2 leads to complete covering of the anodized titanium with the GO/Ca-P coatings. However, these coatings demonstrate poor quality and tracks of bubbling in some regions (marked with yellow arrows). As mentioned before, the gaseous bubbles produced because of water reduction during electrodeposition, in their own turn, could deteriorate the adhesion of the coating to the substrate [12,13]. Hence, poor quality and weak adhesion of the coatings applied at 10 and 15 mA/cm^2 can be as a consequence of producing a large amount of H_2 bubbles due to the further reduction of water base electrolyte at such high current densities.

Therefore, it has been attempted to provide the enough time for escaping H_2 gases with increasing the off time of the pulsed current. Our investigations show that the co-electrodeposition under the duty cycle of 0.1 (t_{on}:1s and t_{off}:9s) results in formation of a uniform and crack free GO/Ca-P coating with an acceptable quality. In this duty cycle, the bonding strength of the GO/Ca-P coatings applied at 10 and 15 mA/cm^2 to the anodized titanium are also measured to be 16±1.8 and 14.2 ±1.2 MPa, respectively.

Fig. 7 shows the cross sectional images of the Ca-P and GO/Ca-P coatings applied at the current densities of 10 and 15 mA/cm^2 and the duty cycle of 0.1. According to these images, the thickness of the GO/Ca-P coating is always lower than the Ca-P one, mainly owing to reduction of the electrodeposition rate in the presence of GO sheets.

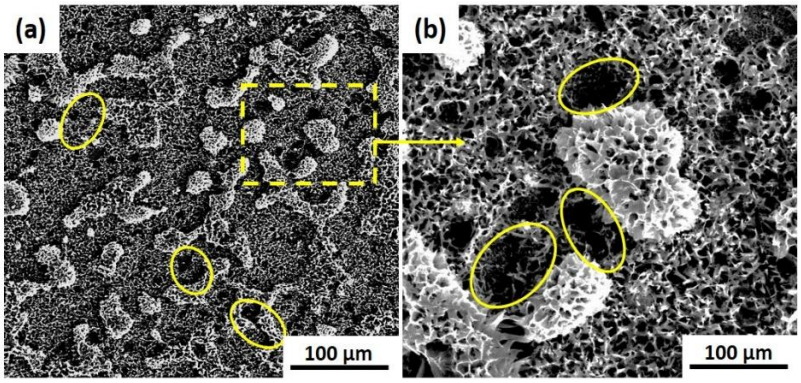

Fig. 5- The SEM micrographs with low and higher magnification (a and b, respectively) for the GO/Ca–P coating deposited at the constant current density of 5 mA/cm^2 and the duty cycle of 0.3 for 60 min.

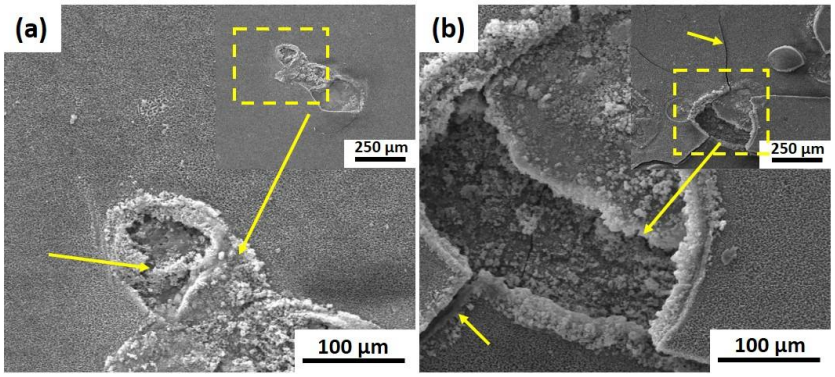

Fig. 6- The SEM micrographs of the GO/Ca-P coatings applied at the duty cycle of 0.3 and the current density of (a) 10 and (b) 15 mA/cm^2.

Moreover, a more growing in the thickness of this composite coating is obtained comparing to that of the Ca-P one by raising the current density from 10 to 15 mA/cm^2. Therefore, it can be concluded that applying the higher current density leads to more increasing in the electrodeposition rate of the GO/Ca-P composite coating as compared to the Ca-P coating.

Up to now, numerous theories have been reported for co-electrodeposition mechanism including connective diffusion, adsorption and electrophoresis [17]. The following is a review of these mechanisms.

The incorporation of particles into the coating consists three steps of i) transport of ions and particles to the surface, ii) loose adsorption and iii) irreversible incorporation of particles by reduction of the ions adsorbed on their surface [18]. When particles are available as the second phase in the electrolyte, the mechanism of co-electrodeposition could be diffusion-controlled because of the transfer of these particles [19]. Regarding this, the size of particles influences their incorporation into the deposit and the co-electrodeposition rate. A large difference between the size of ions and particles causes they diffuse with different diffusion coefficient [18]. When the size increases, the amount of particles which are incorporated into the coating decreases owing to need a more time for reaching and adhesion of larger particles to the electrode surface [17]. Moreover, Whithers proposed that the charged particles are drawn to the electrode surface by electrostatic forces. Valdes also considered electrophoretic transport, which is the response of an electrical field [20]. In fact, by increasing the current density, the charged particles move and adsorb faster to the polarized surface as a result of producing the stronger electrostatic forces [21]we report on the successful incorporation of non-covalently functionalized multi-wall carbon nanotubes (MWCNTs). Then, these particles lose their adsorbed ions and strongly adhere to this polarized surface. Hence, when the matrix of the composite coating is deposited onto the substrate, the particles as the second phase are incorporated into this growing coating due to reduction of the ions adsorbed on their surface [14].

The electrolyte used in the current study for applying the Ca-P coatings is containing only single calcium and phosphate ions (Fig. 8a). These ions

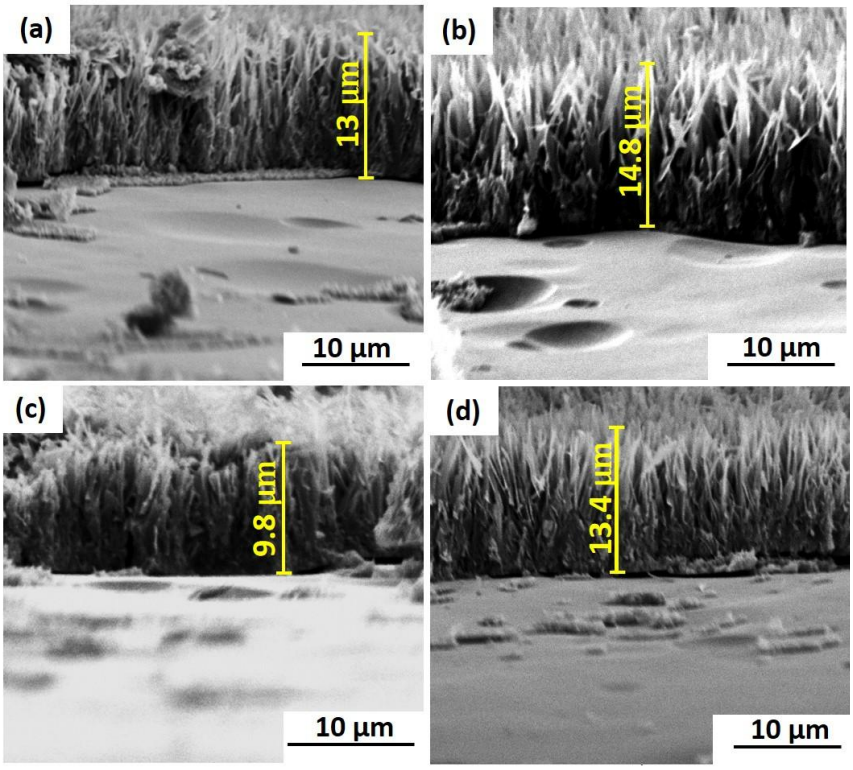

Fig. 7- The cross-sectional images for different coatings of a) Ca-P, 10 mA/cm^2, b) Ca-P, 15 10 mA/cm^2 C) GO/Ca-P, 10 mA/cm^2 and d) GO/Ca-P 15 mA/cm^2.

can easily move towards the cathodically polarized surface even under the relatively weak electrostatic forces at the low current densities. However, for co-electrodeposition of the GO/Ca-P composite coating, besides the calcium and phosphate ions, the suspended particles of GO are available in the electrolyte. The functional groups on GO sheets can interact with a portion of calcium and phosphate ions in the electrolyte [22] to form the GO-ions complexes (see Fig. 8b).

Indeed, diffusion rate of the ions adsorbed on these complexes is dependent on the mass transport of GO sheets to the cathodically polarized surface. It is well known that GO sheets have a high specific surface area up to 2630 m^2g^{-1} [22]. Since size of the GO-containing complexes is larger than distinct calcium and phosphate ions; therefore, these complexes can diffuse and adsorb to the cathode surface with slower rates, causing a decrease in the co-electrodeposition rate of the GO/Ca-P composite coating. This is evident from the comparison of the weight and thickness of the Ca-P and GO/Ca-P coatings applied under the same conditions. Additionally, in low current densities, the electrostatic forces are not adequate for proper mass transport and adsorption of complexes to the cathode. Consequently, only single calcium and phosphate ions along with a small number of complexes, which are reached to the vicinity of the polarized surface, can participate in the co-electrodeposition process. As a result, the rate of co-electrodeposition at the low current densities of 2 and 5 mA/cm^2 significantly reduces and the obtained coatings have poor ability to cover the whole surface of anodized titanium (see Fig.4 c, d). In contrast to this, the stronger electrostatic forces at higher current densities accelerate the mass transport and adsorption of the complexes to the cathode surface. As a result, the co-electrodeposition rate of the GO/Ca-P composite coating increases by applying the higher current densities of 10 and 15 mA/cm^2, and therefore, the coverage capability of this coating can improve. Under this condition, the differences between the coating weight and thickness of the Ca-P and GO/Ca-P coatings reduce, although the values of weight and thickness measured for the composite coatings are still lower.

Fig. 9 displays FTIR spectra of the synthesized GO, as well as the Ca-P and GO/Ca-P coatings applied at the current densities of 10 and 15 mA/cm^2 and duty cycle of 0.1. The spectrum of GO in Fig. 9 (a) shows the bands located at 1053, 1252, 1408 and 1721 cm^{-1} corresponded to the stretching vibration of C–O, C-O-C, C–OH and C=O, respectively. The presence of these oxygen-containing groups proves the successful oxidation of graphite during synthesis of GO. Also, the band at 1625 cm^{-1} is related to the C=C stretching of un-oxidized graphitic domains in the GO phase [23]. Meanwhile, in the FTIR spectra of the coatings (Figs. 9 (b-e)), there are the bands at 474,564, 602, 972, 1031 and 1086 cm^{-1} assigned to phosphate groups (PO_4^{3-}), indicating the formation of a well-

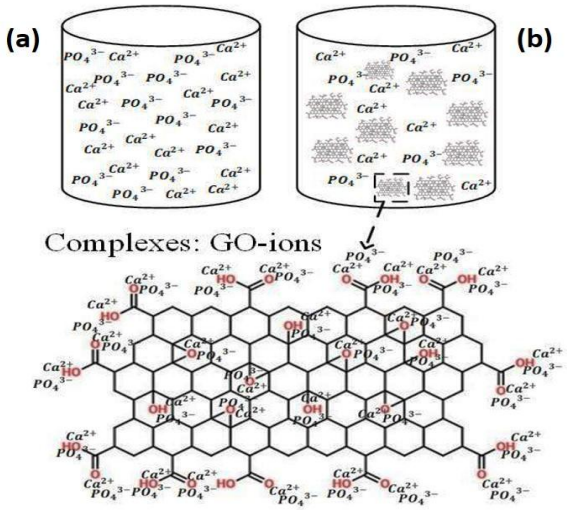

Fig. 8- Schematic illustration of the ions and GO-ions complexes in the electrolyte used for applying a) Ca-P and b) GO/Ca-P coatings.

crystallized HA phase [8,24]. The weak or shoulder peaks at 525, 1075, and 1110 cm^{-1} are also attributed to the hydrogen phosphate groups (HPO_4^{2-}), suggesting the deposition of the other calcium phosphate phases like octacalcium phosphate (OCP) and brushite (dicalcium phosphate dehydrate: DCPD) [7,25]. The additional peaks at 870, 1390 cm^{-1} and between 1400-1500 cm^{-1} show the partial substitution of CO_3^{2-} in the HA structure and so formation of the carbonated hydroxyapatite (CHA) as a dominant phase in both Ca-P and GO/Ca-P coatings [7,25]. The source of these carbonates is CO_2 gases dissolved from atmosphere into the electrolyte during electrodeposition process. It has been reported that the carbonated type of HA is more similar to biological apatite and hence it is very useful for biomedical applications [26]the mechanical and biological properties of Ni-doped hydroxyapatite (HA. Other rest bands at 1625, 1645, and 1672 cm^{-1} are corresponded to the adsorbed water [8,22].

Comparing the results reveals that increasing the current density to 15 mA/cm^2 could be more favorable to form the HA phase. In fact, reduction of water on the cathode surface according to reaction (1) provides the alkaline condition required for electrocrystallization [27].

$$2H_2O + 2e^- \rightarrow 2OH^- + H_2 \quad \text{(eq. 1)}$$

A sufficient concentration of OH^- and PO_4^{3-} is needed to deposit HA phase through reaction (2) [5,27]:

$$10Ca^{2+} + 6PO_4^{3-} + 2OH^- \rightarrow Ca_{10}(PO_4)_6(OH)_2\,(HA) \quad \text{(eq. 2)}$$

However, the hydrogen phosphates could not be fully converted to phosphates if pH is not high enough. Under this condition, other calcium phosphate phases like OCP and brushite can be deposited by reactions (3) and (4), respectively [27,28]:

$$Ca^{2+} + HPO_4^{2-} + 2H_2O \rightarrow CaHPO_4.\ 2H_2O\ \text{(brushite)} \quad \text{(eq. 3)}$$

$$8Ca^{2+} + 2HPO_4^{2-} + 4\,PO_4^{3-} + 5\,H_2 \rightarrow Ca_8H_2(PO_4)_6.5H_2O\ (OCP) \quad \text{(eq. 4)}$$

Considering the biomedical applications, among all Ca-P phases, HA is the most stable [29] and biocompatible [12] phase during implantation into the host body. Therefore, deposition of HA is preferred than the other Ca-P phases. Increasing the current density to 15 mA/cm^2 results in the further reduction of water (reaction (1)). Consequently, producing a higher amount of hydroxyl ions could provide the appropriate condition for nucleation and growth of HA crystals. Moreover, based on

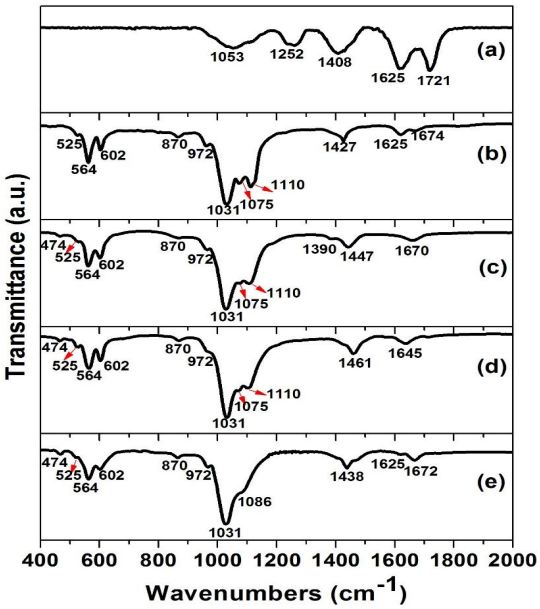

Fig. 9- FTIR spectra of (a) the synthesized GO, and the coatings: (b) Ca-P; 10 mA/cm^2, (c) Ca-P; 15 mA/cm^2, (d) GO/Ca-P; 10 mA/cm^2, and (e) GO/Ca-P; 15 mA/cm^2.

the FTIR results, in the presence of GO sheets the formation of HA phase becomes more possible. In this regard, the bands corresponded to OCP and brushite phases at 1075 and 1110 cm^{-1} are disappeared in the FTIR spectrum of the GO/Ca-P coating electrodeposited at 15 mA/cm^2 (see Fig. 9e). One reason for this result is the effective role of abundant oxygen-containing functional groups of GO sheets such as hydroxyl and carboxyl on the nucleation of HA crystals [22,30]. Besides, we believe that the rate of electrodeposition could possibly affect the type of phases formed in the coating. As previously demonstrated, the presence of GO sheets leads to a decrease in the co-electrodeposition rate. This means that there is probably an enough time to produce adequate hydroxyl groups via water reduction before electrocrystallization of the GO/Ca-P coating. Therefore, several factors including the presence of oxygen containing groups such as hydroxyl on the GO sheets, applying the higher current density of 15 mA/cm^2, and the reduction of the co-electrodeposition rate in the presence of GO can provide adequate hydroxyl groups required for nucleation and growth of HA phase in the GO/Ca-P coating.

Fig. 10 illustrates the micro-Raman spectra of the Ca-P and GO/Ca-P coated samples, which are prepared at two different current densities of 10 and 15 mA/cm^2 and the duty cycle of 0.1.

In these spectra, the peaks located at 397, 514 and 635 cm^{-1} are assigned to the anatase phase [7]. This phase is formed because of the heat treatment of the anodized titanium at 500 $^{\circ}C$ and is appeared in the Raman spectra most likely due to the porous structure of the Ca-P based coatings. Moreover, the PO_4^{3-} groups of the HA phase exhibit the peaks at 964, 1010 and 1048 cm^{-1} [7,12]. A low-intensity peak located at 780 cm^{-1} is also observable in the Raman spectrum of the Ca-P coating applied at 10 mA/cm^2, which is indicative of the formation of the OCP-like phase [31]. For the GO/Ca-P coatings, there are two additional bands assigned to the GO phase at 1355 cm^{-1} (D band) and 1597 cm^{-1} (G band) (Figs. 10 (c and d)). The appearance of these bands in Raman spectra indicates the successful incorporation of GO into these composite coatings. Moreover, as can be seen from Figs. 10 (c and d), the intensity of D and G bands increases by raising the current density to 15 mA/cm^2 and the ratio of I (G) / I (PO_4^{3-} at 964 cm^{-1}) reaches from 0.67 to 0.9. This suggests that the more concentration of GO sheets could be incorporated into the GO/Ca-P coatings applied at higher current densities. In fact, during the co-electrodeposition process, hydrophilic particles as the second phase either ride or incorporate into the coating depending on the growth rate. The faster growth rate causes the incorporation of a higher amount of particles [32]. Hence, the riding effect of particles decreases by raising the current density [32,33]. Besides, increasing the amount of GO sheets in the coating applied at higher current density of 15 mA/cm^2 is in consistent with Guglielmi's model, in which the electrical field-assisted adsorption of particles leads to their incorporation into the coating [19]. As mentioned before, the stronger electrostatic forces at the higher current densities leads to the more easily mass transport and adsorption of GO containing complexes to the cathodically polarized surface. The similar results have already been reported by other researchers about the effect of current density on the incorporation of particles into the coating applied by co-electrodeposition process [19,21]we report on the successful incorporation of non-covalently functionalized multi-wall carbon nanotubes (MWCNTs).

According to the results, choosing the appropriate range of current density is very important for the co-electrodeposition of the GO/Ca-P coating. Applying the current densities of 10 and 15 mA/cm^2 causes the formation of more uniform composite coatings, which could completely cover the whole surface of the anodized titanium. Additionally, at the higher current density of 15 mA/cm^2, the formation of more stable phase of HA and incorporation of GO sheets into the coating could be more facilitated.

Figs. 11 (a and b) show the high-magnification SEM micrographs of Ca-P and GO/Ca-P coatings electrodeposited at 15 mA/cm^2 and duty cycle of 0.1, respectively. The GO sheets could not be distinguished clearly in the SEM image of the GO/Ca-P coating, most likely due to the covering of these sheets with Ca-P crystals. A comparison between the morphology of both Ca-P and GO/Ca-P coatings shows that the incorporation of GO sheets results in the formation of a more compact and refined structure. This could be explained by considering the role of oxygen-containing groups of GO in adsorbing the Ca^{2+} ions and subsequently PO_4^{3-} ions via an electrostatic interaction. Therefore, the GO sheets could provide anchoring sites for nucleation of the Ca-P crystals [30]. Moreover, Fig. 11 (c) displays the wrinkled-paper-like morphology

of GO sheets. Comparing Figs. 11 (a-c) shows that the GO sheets have a larger size as compared to the Ca-P crystals as well as the calcium and phosphate ions, which is in good agreement with the schematic of GO-ions shown in Fig. 8.

The ability of bone mineralization is very important to induce the rapid bone healing. Regarding this, the second particles used as the mechanical reinforcing in the Ca-P based coatings should also retain the original biocompatibility of the calcium phosphates (Ca-Ps) such as HA. Therefore, here, we studied the effect of GO adding on biocompatibility of the Ca-P coatings through immersion of the coated samples in SBF solution.

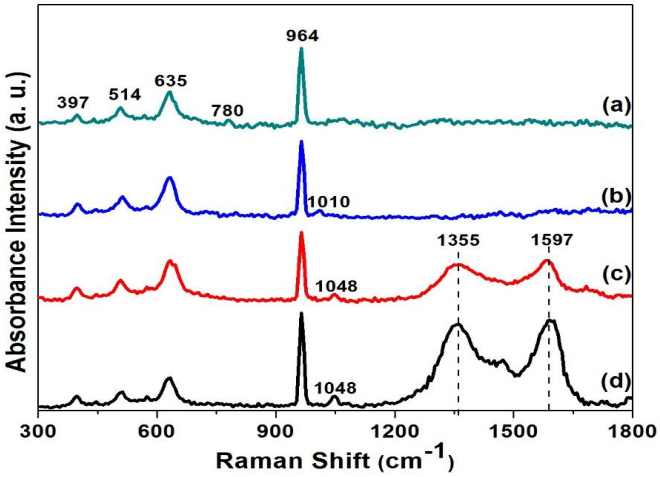

Fig. 10- The micro-Raman spectra of the samples coated with a layer of (a) Ca-P; 10 mA/cm^2, (b) Ca-P; 15mA/cm^2, (c) GO/Ca-P; 10 mA/cm^2, and (d) GO/Ca-P; 15 mA/cm^2.

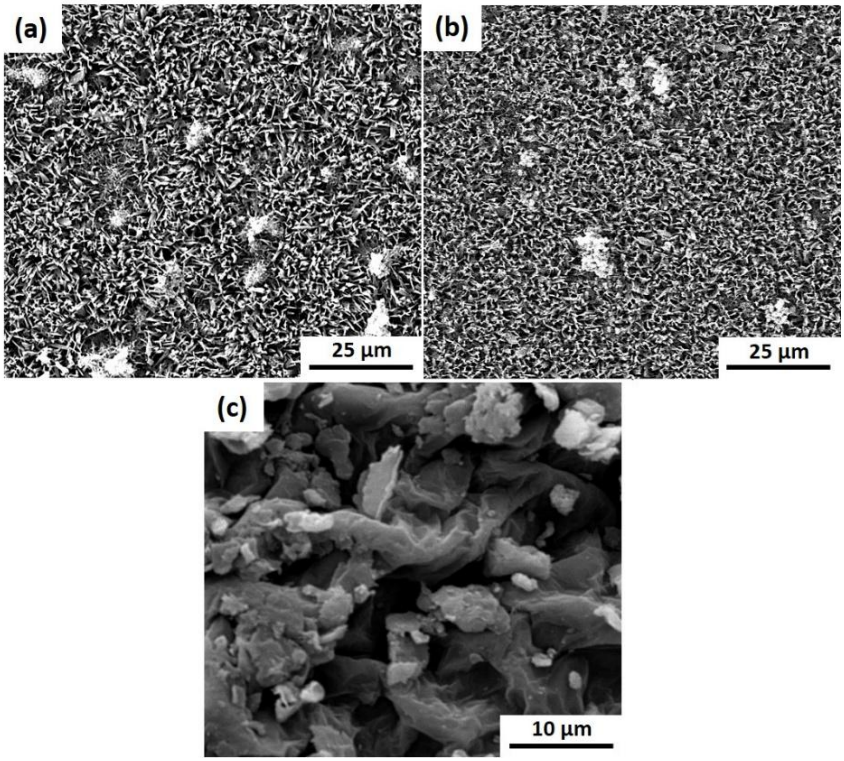

Fig. 11- The surface morphologies of the coatings applied at 15 mA/cm^2 (a) Ca-P, and (b) GO/Ca-P. (c) The SEM image of the synthesized GO.

The SEM micrograph of the Ca-P and GO/Ca-P coatings applied at 15 mA/cm^2 and duty cycle of 0.1 after 7 days of immersion are shown in Figs. 12 (a and b). These images demonstrate that both coatings are covered with the spherical shaped particles of bone-like apatite. The precipitation of these apatite particles from SBF solution on the surface of the coated samples indicates the satisfactory biocompatibility of both coatings. The Ca/P ratio of the apatite-like layer formed on the Ca-P and GO/Ca-P coatings is also measured by the point EDS analysis (Ca% + P% + O% = 100%) to be 1.52 and 1.58, respectively, which are closed to this ratio in the human biological apatite (1.67). Moreover, as can be seen from Fig. 12 (c), the apatite particles could not completely cover the whole surface of the GO/Ca-P coated sample, which is prepared at the current density of 5 mA/cm^2. This is due to the existence of some uncoated areas on the surface of this sample (see Fig. 4d), while, the apatite spheres during 7 days immersion in SBF could be formed only on the areas where the Ca-P based coating is present.

4. Conclusion

In the present study, the surface pretreatment of titanium substrate was done by anodizing. Subsequently, the Ca-P and GO/Ca-P coatings were applied on this anodized surface by the pulsed electrodeposition method at four different current densities of 2, 5, 10 and 15 mA/cm^2. The results showed that the co-electrodeposition of the GO/Ca-P coatings at low current densities of 2 and 5 mA/cm^2 led to remain some uncoated areas on the surface of the anodized titanium. It was because of the large size of GO sheets as compared to calcium and phosphate ions, which in turn caused a decrease in the co-electrodeposition rate of these composite coatings. The better coverage of surface was achieved by increasing the current density to 10 and 15 mA/cm^2. However, the quality of the resulting coatings reduced as a consequence of a high amount of H_2 bubbles evolved at the surface during the co-electrodeposition. To overcome this problem, the off time of the pulsed current increased with changing the duty cycle from 0.3 to 0.1. Under this condition, the GO/Ca-P coatings with acceptable quality and better surface coverage were formed at 10 and 15 mA/cm^2. Meanwhile, the GO/Ca-P coating applied at 15 mA/cm^2 predominantly consisted of the HA phase and a higher concentration of GO sheets as compared to this coating which was prepared at 10 mA/cm^2. The SEM images demonstrated that in the presence

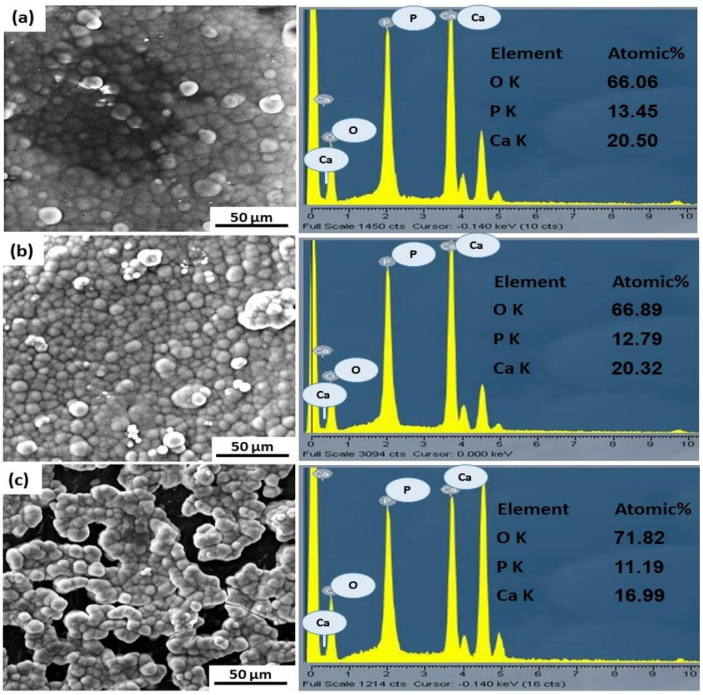

Fig. 12- The SEM images and EDS analysis taken from the coated samples after their immersion in SBF at 37 °C for 7 days: (a) Ca-P; 15 mA/cm^2, (b) GO/Ca-P; 15 mA/cm^2, and (c) GO/Ca-P; 5 mA/cm^2.

of GO sheets a more compact coating could be achieved. Indeed, the negatively charged GO sheets could provide the nucleation sites and facilitate the formation of HA phase. Finally, both Ca-P and GO/Ca-P coatings applied at 15 mA/cm^2 revealed the good biocompatibility as a result of the formation of apatite spheres on their whole surface during 7 days immersion in SBF solution.

References

1. Parcharoen Y, Kajitvichyanukul P, Sirivisoot S, Termsuksawad P. Hydroxyapatite electrodeposition on anodized titanium nanotubes for orthopedic applications. Applied Surface Science. 2014;311:54-61.
2. Blackwood DJ, Seah KHW. Galvanostatic pulse deposition of hydroxyapatite for adhesion to titanium for biomedical purposes. Materials Science and Engineering: C. 2010;30(4):561-5.
3. Yan Y, Zhang X, Mao H, Huang Y, Ding Q, Pang X. Hydroxyapatite/gelatin functionalized graphene oxide composite coatings deposited on TiO2 nanotube by electrochemical deposition for biomedical applications. Applied Surface Science. 2015;329:76-82.
4. Lee K, Jeong Y-H, Brantley WA, Choe H-C. Surface characteristics of hydroxyapatite films deposited on anodized titanium by an electrochemical method. Thin Solid Films. 2013;546:185-8.
5. Raj V, Mumjitha MS. Fabrication of biopolymers reinforced TNT/HA coatings on Ti: Evaluation of its Corrosion resistance and Biocompatibility. Electrochimica Acta. 2015;153:1-11.
6. Janković A, Eraković S, Vukašinović-Sekulić M, Mišković-Stanković V, Park SJ, Rhee KY. Graphene-based antibacterial composite coatings electrodeposited on titanium for biomedical applications. Progress in Organic Coatings. 2015;83:1-10.
7. Fathyunes L, Khalil-Allafi J. Characterization and corrosion behavior of graphene oxide-hydroxyapatite composite coating applied by ultrasound-assisted pulse electrodeposition. Ceramics International. 2017;43(16):13885-94.
8. Fathyunes L, Khalil-Allafi J, Moosavifar M. Development of graphene oxide/calcium phosphate coating by pulse electrodeposition on anodized titanium: Biocorrosion and mechanical behavior. Journal of the Mechanical Behavior of Biomedical Materials. 2019;90:575-86.
9. Li M, Liu Q, Jia Z, Xu X, Cheng Y, Zheng Y, et al. Graphene oxide/hydroxyapatite composite coatings fabricated by electrophoretic nanotechnology for biological applications. Carbon. 2014;67:185-97.
10. Mohajernia S, Hejazi S, Eslami A, Saremi M. Modified nanostructured hydroxyapatite coating to control the degradation of magnesium alloy AZ31 in simulated body fluid. Surface and Coatings Technology. 2015;263:54-60.
11. Benea L, Mardare-Danaila E, Celis J-P. Increasing the tribological performances of Ti–6Al–4V alloy by forming a thin nanoporous TiO2 layer and hydroxyapatite electrodeposition under lubricated conditions. Tribology International. 2014;78:168-75.
12. Fathyunes L, Khalil-Allafi J, Sheykholeslami SOR, Moosavifar M. Biocompatibility assessment of graphene oxide-hydroxyapatite coating applied on TiO 2 nanotubes by ultrasound-assisted pulse electrodeposition. Materials Science and Engineering: C. 2018;87:10-21.
13. Fathyunes L, Khalil-Allafi J. Effect of employing ultrasonic waves during pulse electrochemical deposition on the characteristics and biocompatibility of calcium phosphate coatings. Ultrasonics Sonochemistry. 2018;42:293-302.
14. Hovestad A, Janssen LJJ. Electroplating of Metal Matrix Composites by Codeposition of Suspended Particles. Modern Aspects of Electrochemistry: Springer-Verlag. p. 475-532.
15. Walsh FC, Ponce de Leon C. A review of the electrodeposition of metal matrix composite coatings by inclusion of particles in a metal layer: an established and diversifying technology. Transactions of the IMF. 2014;92(2):83-98.
16. Fathyunes L, Khalil-Allafi J. The effect of graphene oxide on surface features, biological performance and bio-stability of calcium phosphate coating applied by pulse electrochemical deposition. Applied Surface Science. 2018;437:122-35.
17. Low CTJ, Wills RGA, Walsh FC. Electrodeposition of composite coatings containing nanoparticles in a metal deposit. Surface and Coatings Technology. 2006;201(1-2):371-83.
18. Nasirpouri F. Electrodeposition of Nanostructured Materials. Springer Series in Surface Sciences: Springer International Publishing; 2017.
19. Das MK, Li R, Qin J, Zhang X, Das K, Thueploy A, et al. Effect of electrodeposition conditions on structure and mechanical properties of Ni-W/diamond composite coatings. Surface and Coatings Technology. 2017;309:337-43.
20. Vb S. An Overview on the Preparation, Characterization and Properties of Electrodeposited-Metal Matrix Nanocomposites. Nanoscience & Technology: Open Access. 2014;1(3).
21. Daneshvar-Fatah F, Nasirpouri F. A study on electrodeposition of Ni-noncovalnetly treated carbon nanotubes nanocomposite coatings with desirable mechanical and anti-corrosion properties. Surface and Coatings Technology. 2014;248:63-73.
22. Baradaran S, Moghaddam E, Basirun WJ, Mehrali M, Sookhakian M, Hamdi M, et al. Mechanical properties and biomedical applications of a nanotube hydroxyapatite-reduced graphene oxide composite. Carbon. 2014;69:32-45.
23. Krishnamoorthy K, Veerapandian M, Yun K, Kim SJ. The chemical and structural analysis of graphene oxide with different degrees of oxidation. Carbon. 2013;53:38-49.
24. Garskaite E, Gross K-A, Yang S-W, Yang TC-K, Yang J-C, Kareiva A. Effect of processing conditions on the crystallinity and structure of carbonated calcium hydroxyapatite (CHAp). CrystEngComm. 2014;16(19):3950.
25. Utku FS, Seckin E, Goller G, Tamerler C, Urgen M. Carbonated hydroxyapatite deposition at physiological temperature on ordered titanium oxide nanotubes using pulsed electrochemistry. Ceramics International. 2014;40(10):15479-87.
26. Baradaran S, Moghaddam E, Nasiri-Tabrizi B, Basirun WJ, Mehrali M, Sookhakian M, et al. Characterization of nickel-doped biphasic calcium phosphate/graphene nanoplatelet composites for biomedical application. Materials Science and Engineering: C. 2015;49:656-68.
27. Gopi D, Indira J, Kavitha L. A comparative study on the direct and pulsed current electrodeposition of hydroxyapatite coatings on surgical grade stainless steel. Surface and Coatings Technology. 2012;206(11-12):2859-69.
28. Kar A, Raja KS, Misra M. Electrodeposition of hydroxyapatite onto nanotubular TiO2 for implant applications. Surface and Coatings Technology. 2006;201(6):3723-31.
29. Saremi M, Mohajernia S, Hejazi S. Controlling the degradation rate of AZ31 Magnesium alloy and purity of nano-hydroxyapatite coating by pulse electrodeposition. Materials Letters. 2014;129:111-3.
30. Mahto TK, Chandra Pandey S, Chandra S, Kumar A, Sahu Sk. Hydroxyapatite conjugated graphene oxide nanocomposite: a new sight for significant applications in adsorption. RSC Advances. 2015;5(117):96313-22.
31. Lobo AO, Corat MAF, Ramos SC, Matsushima JT, Granato AEC, Pacheco-Soares C, et al. Fast Preparation of Hydroxyapatite/Superhydrophilic Vertically Aligned Multiwalled Carbon Nanotube Composites for Bioactive Application. Langmuir. 2010;26(23):18308-14.
32. Stappers L, Fransaer J. AFM Study of the Incorporation of Particles during Electrodeposition. Journal of The Electrochemical Society. 2007;154(11):D598.
33. Stappers L, Fransaer J. Growth of Metal around Particles during Electrodeposition. Journal of The Electrochemical Society. 2006;153(7):C472.